Size effects in the thermal conductivity of gallium oxide (β-Ga2O3) films grown via open-atmosphere annealing of gallium nitride

Chester J. Szwejkowski, Nicole C. Creange, Kai Sun, Ashutosh Giri, Brian F. Donovan, Costel Constantin, and Patrick E. Hopkins

Citation: Journal of Applied Physics **117**, 084308 (2015); doi: 10.1063/1.4913601
View online: http://dx.doi.org/10.1063/1.4913601
View Table of Contents: http://scitation.aip.org/content/aip/journal/jap/117/8?ver=pdfcov
Published by the AIP Publishing

Size effects in the thermal conductivity of gallium oxide (β-Ga_2O_3) films grown via open-atmosphere annealing of gallium nitride

Chester J. Szwejkowski,[1] Nicole C. Creange,[2] Kai Sun,[3] Ashutosh Giri,[1] Brian F. Donovan,[1] Costel Constantin,[2,a)] and Patrick E. Hopkins[1,b)]
[1]*Department of Mechanical and Aerospace Engineering, University of Virginia, Charlottesville, Virginia 22904, USA*
[2]*Department of Physics and Astronomy, James Madison University, Harrisonburg, Virginia 22807, USA*
[3]*Department of Materials Science and Engineering, University of Michigan, Ann Arbor, Michigan 48109, USA*

(Received 1 October 2014; accepted 14 February 2015; published online 25 February 2015)

Gallium nitride (GaN) is a widely used semiconductor for high frequency and high power devices due to of its unique electrical properties: a wide band gap, high breakdown field, and high electron mobility. However, thermal management has become a limiting factor regarding efficiency, lifetime, and advancement of GaN devices and GaN-based applications. In this work, we study the thermal conductivity of beta-phase gallium oxide (β-Ga_2O_3) thin films, a component of typical gate oxides used in such devices. We use time domain thermoreflectance to measure the thermal conductivity of a variety of polycrystalline β-Ga_2O_3 films of different thicknesses grown via open atmosphere annealing of the surfaces of GaN films on sapphire substrates. We show that the measured effective thermal conductivity of these β-Ga_2O_3 films can span 1.5 orders of magnitude, increasing with an increased film thickness, which is indicative of the relatively large intrinsic thermal conductivity of the β-Ga_2O_3 grown via this technique ($8.8 \pm 3.4\,W\,m^{-1}\,K^{-1}$) and large mean free paths compared to typical gate dielectrics commonly used in GaN device contacts. By conducting time domain thermoreflectance (TDTR) measurements with different metal transducers (Al, Au, and Au with a Ti wetting layer), we attribute this variation in effective thermal conductivity to a combination of size effects in the β-Ga_2O_3 film resulting from phonon scattering at the β-Ga_2O_3/GaN interface and thermal transport across the β-Ga_2O_3/GaN interface. The measured thermal properties of open atmosphere-grown β-Ga_2O_3 and its interface with GaN set the stage for thermal engineering of gate contacts in high frequency GaN-based devices. © *2015 AIP Publishing LLC*. [http://dx.doi.org/10.1063/1.4913601]

I. INTRODUCTION

As the characteristic times and lengths of devices decrease to scales on the order of the carrier scattering rates and mean free paths, thermal management of material boundaries can become a critical aspect of design.[1–3] In this regime, the energy transport mechanisms that are intrinsic to the materials comprising the device can contribute much less to the overall thermal resistance of the system as compared to the resistances across the individual interfaces. The efficacy of transmitting energy across these solid interfaces can be quantified via the thermal boundary conductance,[4] or Kapitza Conductance,[5] (the inverse of which is the thermal boundary resistance or Kapitza Resistance), and is the constant of proportionality that relates the heat flux to the temperature drop across this interfacial region, mathematically expressed as $h_K = q/\Delta T$, where h_K is the thermal boundary conductance, q is the thermal flux, and ΔT is the interfacial temperature drop.[4] The range of phonon-dominated thermal boundary conductances between solids at room temperature span roughly two orders of magnitude from ~5 to 500 $MW\,m^{-2}\,K^{-1}$, and can be strongly related to the atomic structure and chemistry around the interface.[6] To put this into perspective, this energy transport pathway can offer the equivalent thermal resistance as roughly 300–3.0 nm of high quality SiO_2, respectively. Given the wide spread use of thin gate oxides and additional sacrificial layers in electronic nanodevices, the addition of this thermal resistance associated with interfaces can be highly detrimental to device operation and reliability.

Interfacial thermal engineering has emerged as a solution to bottlenecks in development of high power devices.[7] Where the processor industry has hit roadblocks in maintaining Moore's Law from on chip power densities exceeding 100 $W\,cm^{-2}$ (higher than a typical lab hotplate),[7] even greater power densities have been observed in radio frequency (RF) amplifier gallium nitride-based (GaN) devices.[8,9] This increase in power density creates massive hot-spots in GaN active regions, mainly concentrated near the gate contacts, which directly leads to underperformance and eventual failure of these devices. This thermal bottleneck therefore creates a major issue for furthering of GaN-based technologies, such as high-electron-mobility transistors (HEMTs) for high frequency devices, light emitting diodes (LEDs) for energy-efficient illumination, radar technologies (ship-board, airborne, and ground), and high performance space satellites.

Accordingly, engineering of the thermal properties and energy transport mechanisms associated with the GaN gate contacts can elucidate thermal mitigation mechanisms to

a)Email: constacx@jmu.edu
b)Email: phopkins@virginia.edu

improve GaN performance by reducing Joule heating effects attributed with the thermal resistances at these junctions. In a typical GaN device, such as a MOSFET, the thermal resistances associated with this junction will consist of the metal electrode, a high-dielectric constant ("high-*k*") gate oxide, the GaN channel, and the material interfaces at each of these contacts. It is well known that typical gate oxides can have very low thermal conductivities ($\sim$1 W m^{-1} K^{-1}), and can vary greatly depending on the deposition procedure.[10–12] However, the thermal properties of β-Ga_2O_3, a common component of gate oxides in high frequency devices (including GaN),[13–15] are relatively unstudied. Furthermore, the effects of film thickness on the thermal properties of this oxide, corresponding thermal boundary conductances at the β-Ga_2O_3-contact interfaces, and the interfacial morphology effects on thermal transport have never been experimentally determined, which has imposed a significant roadblock in gate-contact thermal mitigation.

In response, we report on the size effects in the thermal conductivity of beta-phase gallium oxide (β-Ga_2O_3) films grown via annealing (0001) GaN surfaces in open atmosphere. We show that open atmosphere annealing of GaN surfaces can create polycrystalline, phase pure films of β-Ga_2O_3 with varying thicknesses. The duration of the GaN-anneal also leads to both surface roughness on the β-Ga_2O_3 and spiking of the β-Ga_2O_3 phase into the GaN. We measure the thermal conductance of the β-Ga_2O_3 films and interfaces in adjunction using time domain thermoreflectance (TDTR). From our measurements, we quantify the thermal boundary conductance across the β-Ga_2O_3/GaN interface to be in close proximity to the previously reported interface conductance inferred for SiO_2/Si interfaces, another common gate oxide/channel interface widely found in several technologies. However, unlike typical gate oxides, we show that the effective thermal conductivity of our polycrystalline β-Ga_2O_3 can span 1.5 orders of magnitude, increasing with an increased film thickness due to size effects from phonon scattering at the β-Ga_2O_3/GaN interface. From this analysis, we determine that the intrinsic thermal conductivity of open atmosphere grown β-Ga_2O_3 is 8.8 $\pm$ 3.4 W m^{-1} K^{-1}, much higher than typical amorphous gate oxides. This study demonstrates the promise of β-Ga_2O_3 grown via open atmosphere anneal of GaN as a potential oxide that can be used to mitigate near-gate hotspots in GaN devices.

II. GALLIUM OXIDE FABRICATION AND CHEMICAL CHARACTERIZATION

The various gallium oxide films fabricated in this study were developed from commercially available, 5 mm $\times$ 5 mm, single-side polished GaN films (3.4 μm) on sapphire substrates (430 μm) obtained from University Wafer. The GaN films have a Wurtzite crystal structure and are unintentionally n-type doped. To ensure a clean surface prior to annealing, the samples were ultrasonicated for 20 min. in acetone, 20 min. in isopropanol, 20 min. in deionized water, and then dried with inert air. Following this cleaning procedure, we annealed the samples in a tube furnace subjected to a wide variety of annealing conditions, adapted and modified from previous procedures.[16–18] Samples were annealed in 10 min. cycles between 900–1050 °C. This initiated not only growth of gallium oxide[19,20] but also varying degrees of roughness at both the surface of the gallium oxide and the gallium oxide/GaN interface, as observed previously.[21–23] The surface roughness of the gallium oxide was determined using a combination of atomic force microscopy (AFM, Veeco DI Multimode IIIa) and mechanical profilometry. We also approximated the grain size of the Ga_2O_3 layer using AFM images and the linear intercept method to verify that the grain size is larger than the film thickness. The unannealed samples (which were the smoothest) had RMS roughness values (R_q) as low as 0.5 nm, while the roughest sample had R_q over 70 nm with many intermediate roughnesses in between (c.f., Figs. 1(a)–1(h)). The roughness and compositional variance on the GaN surface where growth was initiated were observed with transmission electron microscopy (TEM) and scanning transmission electron microscopy (STEM). The TEM and STEM images reveal that annealing not only caused growth of a rough oxide layer but also changed the compositional abruptness of the Ga_2O_3/GaN interface. Roughness and "spiking" at the interface can be seen in the TEM and STEM images presented in Figs. 1(i)–1(n). Table I summarizes the Ga_2O_3 thicknesses and surface roughnesses determined from the AFM, TEM, and STEM measurements.

The chemistry of the oxide layer was determined using x-ray diffraction (XRD) and x-ray photoelectron spectroscopy (XPS). In Figs. 2(a)–2(d), we present the XRD spectra taken in the range of $2\theta = 20°$–$130°$ as a function of R_q obtained from a PANalytical X'Pert PRO MPD θ-2θ diffractometer with x-ray radiation of Cu ($\lambda = 1.54060$ Å for Cu K_α peak). The signature GaN peaks are observed at 34.39(3)° (0002), 72.69(8)° (0004), and 125.89(1)° (0006). The Sapphire peaks are observed at 41.63(1)° (0006), and 90.49(7)° (00012). The other peaks observed at $2\theta = 31.16(6)°$, 38.32(6)°, and 59.02 (2)° correspond to crystallographic planes of (002), (202), and (113) for β-Ga_2O_3. These β-Ga_2O_3 layers are polycrystalline and form crystallites that have single crystal monoclinic structure, as determined via the AFM, TEM, STEM, and XRD. According to structure factor calculations, the Miller Indices for such monoclinic structures should obey $h + k = 2n$ with $n = 1, 2, 3, 4, \ldots \infty$. The *d*-spacing for a monoclinic crystal structure is calculated according to

$$\frac{1}{d^2} = \frac{1}{\sin^2(\beta)}\left[\frac{h^2}{a^2} + \frac{k^2\sin^2(\beta)}{b^2} + \frac{l^2}{c^2} - \frac{2hl\cos(\beta)}{ac}\right], \quad (1)$$

where *hkl* are the Miller Indices, *abc* are the unit cell lattice constants, and $\alpha\beta\gamma$ are the unit cell internal angles. Equation (1) was useful to check the Miller indices for our β-Ga_2O_3 layers by using well known values for *a*, *b*, and *c* as found in the literature.[24] With Bragg's law [i.e., $n\lambda = 2d\sin(\theta)$], we determined the *d* lattice spacings to be $d_{002} = 2.867(4)$ Å, $d_{202} = 2.346(6)$ Å, $d_{113} = 1.563(8)$ Å, in excellent agreement with those reported by Lv *et al.* (i.e., $d_{002} = 2.82(9)$ Å, $d_{202} = 2.34(4)$ Å, and $d_{113} = 1.53(3)$ Å).[25] The O_{1s} XPS spectra in Fig. 2(e) are presented as a function of surface roughness for our samples with $R_q = 1.0$, 4.9, 9.7, and 12.7 nm.

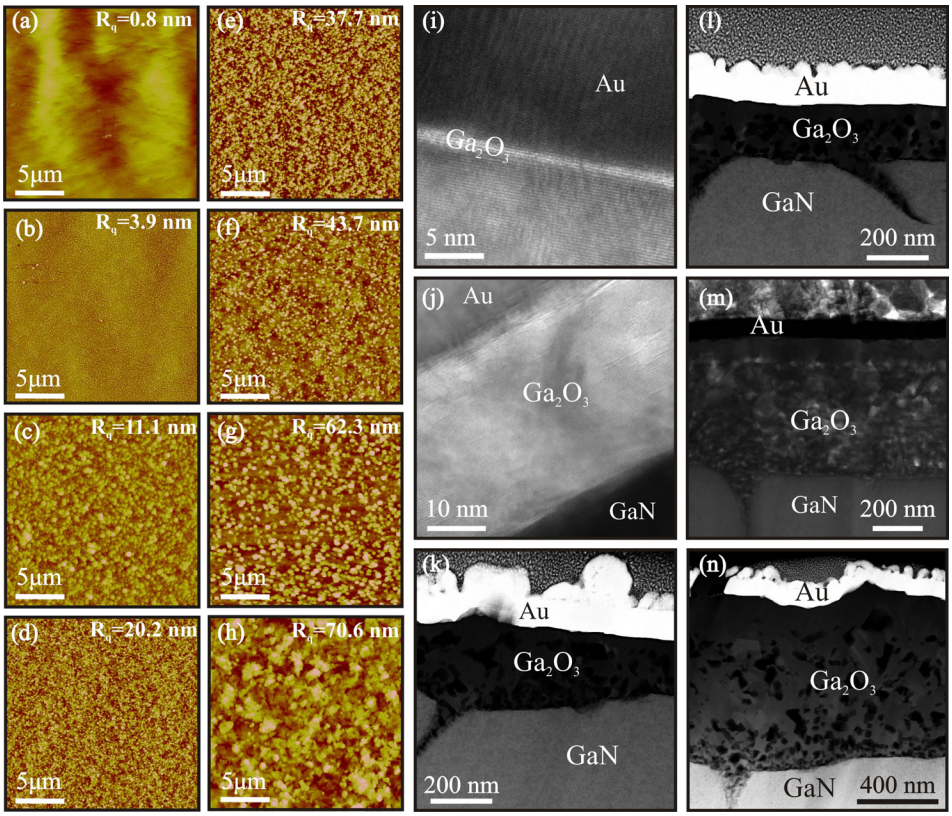

FIG. 1. (a)–(h) Atomic force microscopy images of Ga_2O_3-GaN-Sapphire surfaces for $R_q = 0.8$–70.6 nm. (i), (j), and (m) Cross-sectional high resolution transmission electron microscopy for sample with $R_q = 0.9$–77.2 nm. (k), (l), and (n) High angle annular dark-field images collected in STEM mode for sample with $R_q = 0.9$–77.2 nm.

The binding energies of the examined elements were calibrated using C_{1s} peak (284.6 eV) as a reference. The binding energies for our samples were found to be 534.5 eV ($R_q = 0.5$ nm), 530.50 eV ($R_q = 4.9$ nm), 530.34 eV ($R_q = 9.7$ nm), and 530.15 eV ($R_q = 12.7$ nm). These O_{1s} spectra indicate that the as-received sample (i.e., not annealed and with 0.5 nm RMS roughness—blue curve in Fig. 2) contains a much smaller signature of oxygen compared to the annealed samples; this is consistent with typical thicknesses of native Ga_2O_3 on the GaN surface (i.e., a surface layer of 1–2 nm).[26] It is important to note that as the Ga_2O_3 layer increases in thickness, the O_{1s} shifts towards smaller binding energies, consistent with previous XPS studies showing the effect of the Ga_2O_3 on the GaN spectrum.[27]

We measured the thicknesses of the gallium oxide layer with TEM and STEM, example high-resolution electron micrographs and high angle annular dark-field images of which are presented in Fig. 1(i)–1(n). The TEM and STEM analysis confirms that the increase in surface roughness measured via AFM is directly correlated to an increase in oxide layer thickness. We relate the thickness of gallium oxide to the roughness via a 3rd order polynomial fit (Fig. 3), and use this calibration for analysis of our TDTR measurements, described in more detail below. The error bars in the roughness represent one standard deviation, based on AFM measurements, which are propagated through our polynomial fit to determine the uncertainty in Ga_2O_3 thickness.

For TDTR measurements, we electron-beam evaporate thin metal films on the various Ga_2O_3/GaN samples using metals similar to those employed in electronic devices: 79 nm Au, 78 nm Au with a 2 nm Ti wetting layer, and 89 nm Al. The film thicknesses were verified using a combination

TABLE I. Three sets of samples were fabricated regarding the metal transducer that was deposited. The roughness of the RMS surface of the samples before transducer deposition (R_q) and the thickness of the gallium oxide layer (d) are summarized. Uncertainties in roughness represent one standard deviation of the AFM measurements, while uncertainties in thickness are calculated from our model (Fig. 3) propagating the roughness uncertainty.

Transducer	Au (79 nm)		Al (89 nm)		Au (78 nm)/Ti (2 nm)	
β-Ga_2O_3	R_q (nm)	d (nm)	R_q (nm)	d (nm)	R_q (nm)	d (nm)
	0.9 ± 0.2	2.2 ± 0.4	0.8 ± 0.2	2.2 ± 0.4	0.8 ± 0.2	2.2 ± 0.4
	6.6 ± 0.1	13.2 ± 0.7	4.0 ± 0.1	6.9 ± 0.4	6.9 ± 0.5	14.0 ± 2.7
	11.6 ± 0.4	31.2 ± 3.8	5.0 ± 0.7	9.1 ± 3.0	13.5 ± 0.2	40.2 ± 2.0
	25.9 ± 0.2	124.3 ± 2.7	10.8 ± 1.1	27.9 ± 9.1	33.8 ± 1.6	199.7 ± 34.1
	45.9 ± 2.8	345.7 ± 74.9	14.5 ± 1.0	45.3 ± 11.0	43.2 ± 0.1	310.0 ± 2.8
	60.2 ± 0.5	559.0 ± 18.0	19.4 ± 0.1	74.6 ± 1.2	77.2 ± 1.7	864.0 ± 64.8
	…	…	30.2 ± 0.4	163.3 ± 7.8	…	…
	…	…	41.6 ± 2.1	289.8 ± 52.6	…	…
	…	…	65.6 ± 2.4	651.0 ± 83.2	…	…

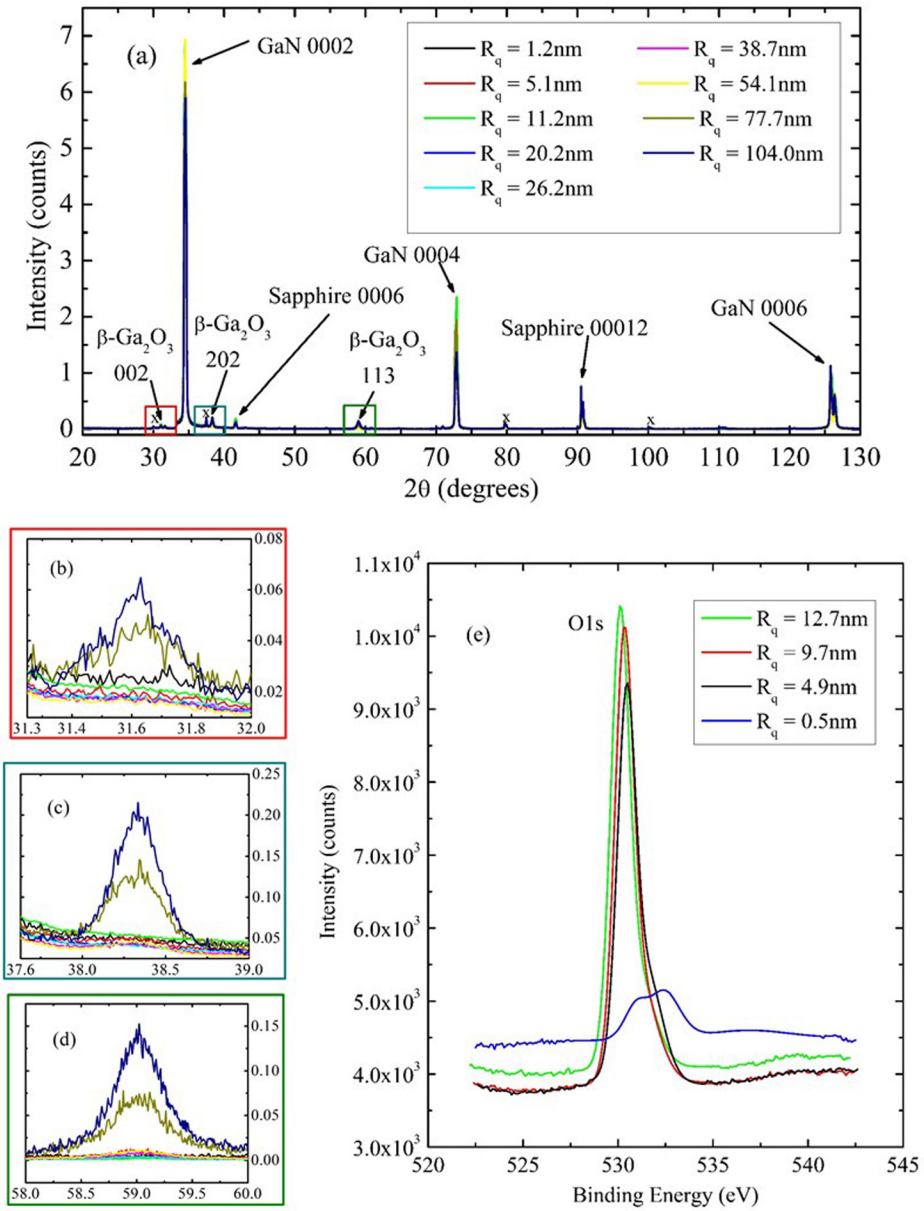

FIG. 2. XRD-XPS. (a) X-ray diffraction (θ-2θ) of β-Ga_2O_3-GaN-Sapphire (0001) thin films as a function of surface roughness root mean square (R_q) for $R_q = 0.9$–104.0 nm. (b)–(d) Scaled up figures for the β-Ga_2O_3 signature peaks (i.e., $2\theta = 31.6°$, $38.3°$, $59.0°$). (e) X-ray photoemission spectroscopy for oxygen O_{1s} peak observed at ~530 eV.

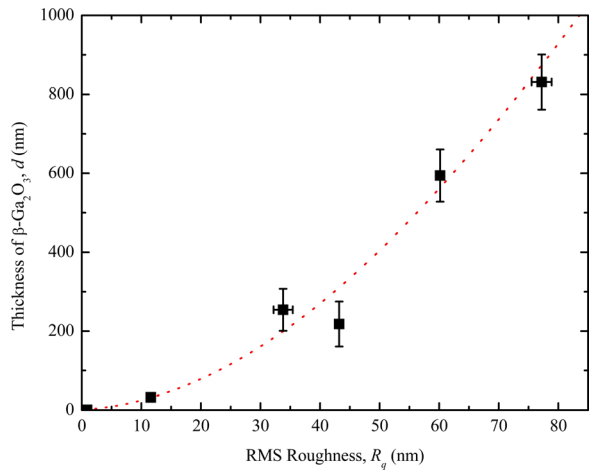

FIG. 3. β-Ga_2O_3 thickness measured via TEM vs. surface roughness measured via AFM. The relationship is modeled by the red dotted line with a third order polynomial equation: $d = -0.0004(R_q)^3 + 0.1667(R_q)^2 + 0.6869(R_q) + 1.5$. This was found to be a statistically sound correlation ($R^2 = 0.975$, $t = 12.6$, $t_{\alpha=0.005} = 4.60$).

of variable angle spectroscopic ellipsometry (VASE from J. A. Woollam) and mechanical profilometry. In the case of the Al film, we were also able to confirm the film thicknesses of most films with picosecond acoustics.[28,29] We report an uncertainty in transducer film thickness of 3 nm. An illustration of sample geometries studied in this work is shown in Fig. 4. Table I summarizes the information for each set of samples.

III. THERMAL CONDUCTIVITY MEASUREMENTS OF THE β-Ga_2O_3 FILMS

The thermal conductivities of the β-Ga_2O_3 films were measured using time domain thermoreflectance (TDTR);[30] pertinent details of TDTR and corresponding data analyses can be found in the literature.[31–33] To briefly summarize, our TDTR experiment is a pump-probe technique utilizing subpicosecond laser pulses that are split into two paths: the pump and probe. The pump pulses are absorbed by the sample and cause a change in the surface temperature on the

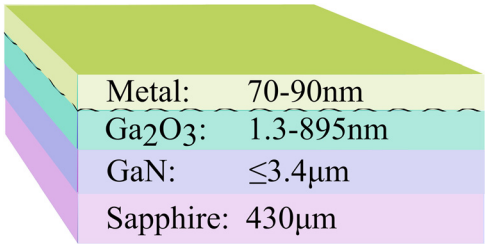

FIG. 4. Illustration of sample geometries studied in this work. The fabrication of our samples includes two stages: the gallium oxide growth and then the metal film deposition. Starting with the commercially available GaN on sapphire, the oxide was grown via open atmosphere annealing for 10 min cycles at temperatures between 900–1050 °C; longer anneals increased the roughness at the oxide surface (indicated by the textured line above the oxide layer). Various metal films were then electron-beam evaporated on top including aluminum, gold, and gold with a titanium adhesion layer.

metal film. This surface temperature decays based on the thermal properties of the materials underneath (in our case, the β-Ga_2O_3 film, the GaN film, the Al_2O_3 substrate, and the associated interfaces) and the temporal change in temperature is subsequently monitored as a function of time via the change in thermoreflectance of the probe pulse.[34–36]

In our specific experiments, we use the sub-picosecond pulses emitted from an 80 MHz Ti:Sapphire oscillator with a central wavelength of 800 nm (~10.5 nm bandwidth) as the basis of our pump-probe experiments. The pump path is modulated at 8.8 MHz, doubled to 400 nm, and focused onto the surface of the metal transducer layer while the thermoreflectivity of the probe path is monitored at the pump frequency with a time-delay of up to 5.5 ns after the initial heating event. The radii of the pump and probe paths are 25 μm and 6.5 μm, respectively, so the heat flow is nearly entirely dominated by cross plane conduction (normal to the interfaces). We used TDTR to characterize the thermal conductance through the β-Ga_2O_3 films and associated interfaces in the three sets of GaN samples (each set is referring to a different metal film transducer). Each set had between six and eight samples with different surface roughnesses based on the annealing conditions, as summarized in Table I. Finally, at least three TDTR scans were performed on each sample to ensure repeatability in our thermal measurements.

The method we use for our data analysis and extracting the effective thermal conductivity of our β-Ga_2O_3 films is described in detail in the literature.[31–33] In short, we fit a multilayer, diffusive thermal model that accounts for the periodic heating of the laser pulses to our TDTR measurements. The inputs to our model analysis require knowledge of the heat capacity, thermal conductivity, and thermal boundary conductance associated with each layer of the system. We used literature values for the heat capacity of GaN (Ref. 37) and β-Ga_2O_3 (Ref. 38) and for the heat capacities and thermal conductivities of Al (Ref. 39) and Au (Ref. 40). At a modulation frequency of 8.8 MHz, the thermal penetration depth in these samples is at most ~2 μm. Thus, we are not sensitive to the thermal properties of the sapphire substrate or thermal boundary conductance across the GaN/sapphire interface. For the as-received samples, we determined across the transducer/GaN interface using a two-layer model (transducer/GaN), treating the nanometer of the β-Ga_2O_3 native oxide as part of the transducer/GaN interface. This measured value for the thermal conductivity of the GaN film was used as a known parameter for analyzing the remaining annealed samples with the same metal transducers. It is important to note that when the thicknesses of the β-Ga_2O_3 films get above a few 10's of nm, the thermal resistance from the metal to the GaN is dominated by the β-Ga_2O_3 and its associated interfaces, and we are relatively insensitive to the thermal conductivity of the GaN.[41] Another assumption in our thermal analyses of the metal/β-Ga_2O_3/GaN samples is that we fix the thermal boundary conductance measured across the transducer/GaN interface in our control (native) samples to be equal to that of the transducer/Ga_2O_3 interface in the annealed samples. For the annealed samples, we used a three-layer model (transducer/β-Ga_2O_3/GaN) to determine the thermal conductivity of the β-Ga_2O_3, where we only fit the thermal conductivity of the β-Ga_2O_3 layer. In this analysis, we assumed that the thermal boundary conductance at the β-Ga_2O_3/GaN interface was very large (i.e., we assumed that this interface offers negligible resistance), so that the measured thermal conductivities of the β-Ga_2O_3 layer from the TDTR measurements are in fact "effective" thermal conductivities that are also influenced by the presence of the β-Ga_2O_3/GaN interface. Therefore, the only parameter that we vary to fit our thermal model to our TDTR data is the thermal conductivity of the β-Ga_2O_3. To simplify our analysis, we ignore grain boundary scattering since the grain sizes are larger than the film thicknesses, making film thickness the limiting dimension. As discussed later, through analyses of the effective thermal conductivities as a function of film thickness, we resolve the intrinsic thermal conductivity of the β-Ga_2O_3 by considering both thermal boundary conductance across the transducer/β-Ga_2O_3 interface[42] and phonon scattering at the β-Ga_2O_3/GaN interface.

Example TDTR data and the corresponding model fit are shown in Fig. 5. We note that there are slight differences in curvature between our best-fit thermal model and the measured data, which we attribute to not fitting for the thermal boundary conductance at the β-Ga_2O_3/GaN interface. As we previously mentioned, we analyze our data based on only fitting one parameter in our thermal model, the thermal conductivity of the β-Ga_2O_3; note, this also exemplifies the power in our procedure as we impose minimal assumptions in our analysis to determine the effective thermal conductivity of the β-Ga_2O_3, and we can use the identical analysis procedure for all samples in this work, regardless of the thicknesses of the β-Ga_2O_3 and varying sensitivities to the β-Ga_2O_3/GaN interface conductance. However, because of this approach, the uncertainties in our reported values are larger than those reported in typical TDTR measurements, discussed below.

The uncertainty in our measurements factors in the repeatability of the measurements and uncertainty in transducer and Ga_2O_3 film thicknesses. From this, the mean uncertainty in our TDTR measurements is ~15%, and up to ~25% for the roughest samples. We note that for R_q above ~50 nm, there are long timescale oscillations, as seen in the right inset of Fig. 5. The long-period oscillations observed in

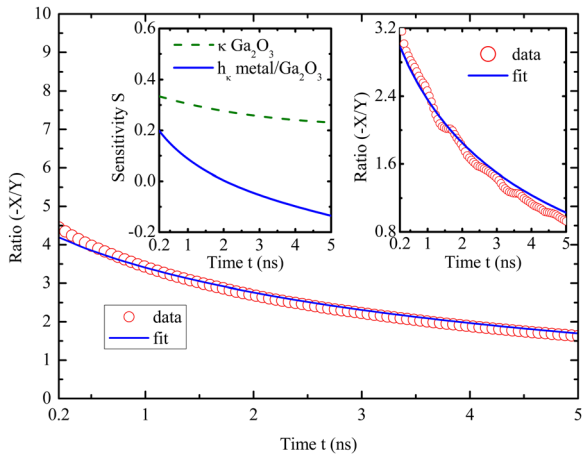

FIG. 5. Thermoreflectance response versus pump-probe delay time. All x-axes are from 0.2 to 5 ns, corresponding to the time regime used to fit for the thermal properties. The large plot and the right inset show the ratio of real and imaginary components of the thermoreflectance response from the lock-in amplifier (-X/Y) as a function of time, and feature the data collected with TDTR (red circles) and the model fit (solid blue line). The large figure is from a relatively smooth sample ($R_q = 6.6$ nm), while the inset is from one of our roughest sample ($R_q = 60$ nm). Note that there are slight differences in curvature between our best-fit thermal model and the measured data, which we attribute to not fitting for the thermal boundary conductance at the β-Ga_2O_3/GaN interface. As discussed in detail in the text, we analyze our data based on only fitting one parameter in our thermal model, the thermal conductivity of the β-Ga_2O_3; Because of this approach, the uncertainties in our reported values are larger than those reported in typical TDTR measurements. In the case of the rough samples (right inset), the long-period oscillations observed could be indicative of thermoelastic effects on the surface of the sample, which are not accounted for in TDTR analyses. Hence, the uncertainty in determining the thermal conductivity for these samples are relatively large, and highlights the limits of using TDTR to measure thermal properties of rough samples. The left inset depicts the sensitivity on the y-axis, showing that from 0.2 to 5 ns, we remain most sensitive to the thermal conductivity of Ga_2O_3 (dashed green line), while less sensitive to the thermal boundary conductance at the transducer/Ga_2O_3 interface (solid blue line) for a rough sample ($R_q = 60$ nm).

these rough samples could be indicative of thermoelastic wave effects on the surface of these samples, which are not accounted for in our TDTR analyses to extract the thermal conductivity of the β-Ga_2O_3 films. Hence, the uncertainties in determining the thermal conductivities of the thicker films with large roughnesses substantially increase. This highlights the limits of using TDTR at these wavelengths to measure thermal properties of rough samples, as once the surface roughness increases above ~50 nm, non-thermal artifacts along with diffusive scattering can skew traditional TDTR analyses. However, we note that even in the roughest sample, we are still sensitive to the thermal conductivity of the Ga_2O_3 film, as exemplified in the left inset of Fig. 5 (here, sensitivity to a parameter is reflected by a large relative magnitude over the pump-probe delay time). To this point, we note that for our thickest and most rough samples, our reported thermal conductivities have larger uncertainties up to ~25% or ± 2.0 W m^{-1} K^{-1}.

IV. RESULTS AND DISCUSSION

The effective thermal conductivities of the gallium oxide films are plotted as a function of film thickness in Fig. 6. Our measurements follow typical thickness-dependent trends reported in the literature for thermal conductivities of other dielectric films both amorphous and crystalline.[3,11,42–45] In the case of the thermal conductivity of the varying thicknesses of amorphous or disordered films, these trends are indicative of the thermal boundary conductance across the film/substrate interface that is included in the measurements of the effective thermal conductivities of the films. However, unlike the thermal conductivities of the amorphous SiO_2 and SiN_x films, the thermal conductivity of β-Ga_2O_3 increases up to thicknesses of several hundred nanometers, approaching 1 μm, with a continued increase in measured thermal conductivity even in the case where our TDTR measurements are insensitive to the β-Ga_2O_3/GaN thermal boundary conductance. This is indicative of the higher intrinsic thermal conductivity of β-Ga_2O_3 and longer phonon mean free paths compared to the amorphous materials resulting in traditional size effects in the thermal conductivity of the β-Ga_2O_3;[3,43] this is not surprising due to the polycrystalline nature of our β-Ga_2O_3 compared to the amorphous SiO_2 and SiN_x films, which—due to the lack of periodicity in their atomic structures—will have intrinsically smaller vibrational mean free paths. The range in measured effective thermal conductivities of the gallium oxide films span 1.5 orders of magnitude; 0.34 W m^{-1} K^{-1} for a film thickness of 12.5 nm up to 8.85 W m^{-1} K^{-1} for a film thickness of 895 nm. The trends are conserved for all three types of samples regarding the metal transducer indicating that there is no appreciable dependence on the transducer.

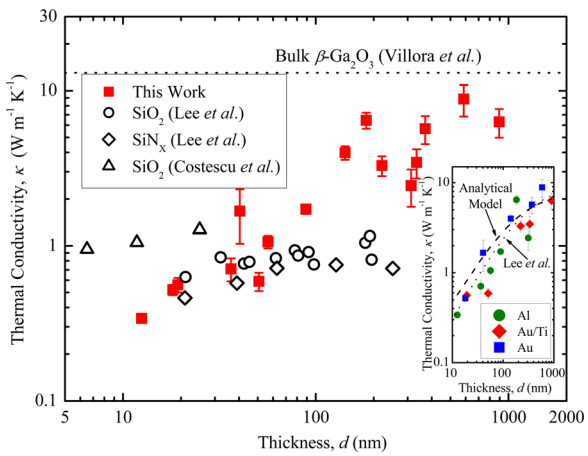

FIG. 6. Measured thermal conductivity as a function of film thickness for our β-Ga_2O_3 films compared to other thin film dielectrics. The thermal conductivity of gallium oxide (filled squares) increases with increased film thickness and approaches the previously reported bulk thermal conductivity (dotted line).[49] This follows the same trend as other dielectric films reported by Lee and Cahill[42] (open circles: SiO_2; diamonds: SiN_x) and Costescu *et al.*[11] (open triangles: SiO_2) and is attributed to boundary scattering. (Inset) Measured thermal conductivity vs. thickness of β-Ga_2O_3 films with the different metal transducers used (filled circles: aluminum; filled diamonds: gold with titanium wetting layer; filled squares: gold), suggesting that the thermal resistance at the transducer/β-Ga_2O_3 is negligible; from this, we conclude that the primary mechanism driving the size effects in the measured thermal conductivities of these films is the thermal resistance associated with the β-Ga_2O_3/GaN interface. The black dotted line is the model used to resolve the thermal boundary conductance across the β-Ga_2O_3/GaN interface, adapted from Lee *et al.*[42] The black dashed line is the analytical model based on phonon thermal conductivity using Umklapp and boundary scattering to account for size effects in thermal conductivity.

From the data in Fig. 6, we can determine the intrinsic thermal conductivity of our β-Ga_2O_3 films through two different modeling approaches that consider different origins of the measured thickness dependence in the effective thermal conductivities of the β-Ga_2O_3 films. The first approach assumes that the reduction in the measured effective thermal conductivity is due to the thermal boundary conductance at the β-Ga_2O_3/GaN interface, which is included in the measured resistance of the β-Ga_2O_3 layer during TDTR analysis. The second approach assumes that the reduction in the β-Ga_2O_3 is due to phonon-boundary scattering leading to size effects in the thermal conductivity. We note that most likely neither approach accurately describes the phonon thermophysics over the entire range of sample thicknesses, but by considering both scenarios, we can improve our accuracy our reported values for the intrinsic thermal conductivity of these β-Ga_2O_3 samples.

Our first approach to analyze the data in Fig. 6 assumes that the thickness dependence in the β-Ga_2O_3 thermal conductivity is an artifact of the thermal boundary conductance across the β-Ga_2O_3/GaN interface being included in the measured effective thermal conductivity extracted from our TDTR measurements. Using the expression presented by Lee and Cahill,[42] the intrinsic thermal conductivity of β-Ga_2O_3 can be derived from our data via

$$\kappa_m = \frac{\kappa_i}{1 + \frac{\kappa_i}{h_\kappa d}}, \tag{2}$$

where κ_m is the measured thermal conductivity, κ_i is the intrinsic thermal conductivity of the β-Ga_2O_3, h_K is the thermal boundary conductance, and d is the thickness of the β-Ga_2O_3. Equation (2) treats the metal/β-Ga_2O_3 thermal conductance, the thermal conductivity of the β-Ga_2O_3 film, and the β-Ga_2O_3/GaN thermal conductance as resistors in series. However, we rule out the inclusion of the resistance across the metal/β-Ga_2O_3 in calculations of Eq. (2) due to the following two reasons: (i) in our TDTR analysis of the thermal conductivity of the β-Ga_2O_3, we only fit the β-Ga_2O_3 thermal conductivity, as we are inherently insensitive to the metal/β-Ga_2O_3 boundary conductance due to the relatively larger resistance of the β-Ga_2O_3 film; and (ii) as shown in the inset of Fig. 6, we do not show any systematic, noticeable dependence in the measured thermal conductivity of the β-Ga_2O_3 for the samples with different metallic transducers. Since we have previously shown that the thermal boundary conductance across these metal films/native β-Ga_2O_3/GaN interfaces can vary by a factor of five depending on the metal film,[41] we conclude that this metal/β-Ga_2O_3 is not contributing to the thermal processes measured in our TDTR experiments. Therefore, the value for thermal boundary conductance in Eq. (2) is representative of the thermal transport across the β-Ga_2O_3/GaN interface. We fit Eq. (2) to our data to extract the thermal conductivity of β-Ga_2O_3 and the thermal boundary conductance across the β-Ga_2O_3/GaN interface (fit shown as dotted line in inset of Fig. 6). From this, we determine a β-Ga_2O_3/GaN thermal boundary conductance of 31.2 ± 8.1 MW m^{-2} K^{-1} and the corresponding intrinsic thermal conductivity of our of open atmosphere-grown β-Ga_2O_3 of 9.7 ± 2.5 W m^{-1} K^{-1}.

The above analysis attributes the reduction in effective thermal conductivity to thermal boundary conductance (suggesting the thermal conductivity of the film is independent of film thickness and the boundary conductance is a byproduct of the measurement). This assumption is clearly not valid for the thicker films where our TDTR measurements are insensitive to the thermal resistance associated with the β-Ga_2O_3/GaN interface. Therefore, we analyze our data using the second approach in which we model our results with a boundary scattering term in the Kinetic Theory-based expression for the thermal conductivity of phonons, given by

$$\kappa = \frac{1}{3}\sum_{j=1}^{3}\int_0^{\omega_{max,j}} \hbar\omega \mathcal{D}_j(\omega)\frac{\partial f_{BE}}{\partial T}v_j^2(\omega)\left(\frac{1}{\tau_i} + \frac{v_j(\omega)}{d}\right)^{-1} d\omega, \tag{3}$$

where $\mathcal{D}$ is the density of states, $\partial f_{BE}/\partial T$ is the temperature derivative of the Bose-Einstein distribution function, v is the phonon group velocity, τ_i is the Umklapp scattering time, and d is the film thickness. The subscript j denotes the branch in the phonon dispersion for the summation. We use a sine-type phonon dispersion for the three acoustic branches of Ga_2O_3 and literature values for frequencies at the Brillouin Zone edge ($\omega_{max,j} = 3.60$ THz, 4.14 THz, and 4.44 THz)[46] and the lattice constant ($a = 5.80$ Å)[46]

$$\omega(\mathrm{k}) = \omega_{max}\sin\frac{\mathrm{k}a}{2}, \tag{4}$$

or, solving for k,

$$\mathrm{k}(\omega) = \frac{2}{a}\sin^{-1}\frac{\omega}{\omega_{max}}. \tag{5}$$

This allows us to write the velocity and density of states as functions of frequency

$$v(\omega) = \frac{\omega_{max}a}{2}\sqrt{1 - \left(\frac{\omega}{\omega_{max}}\right)^2}, \tag{6}$$

$$\mathcal{D}(\omega) = \frac{4\left[\sin^{-1}\frac{\omega}{\omega_{max}}\right]^2}{\pi\omega_{max}a^3\sqrt{1 - \left(\frac{\omega}{\omega_{max}}\right)^2}}. \tag{7}$$

Using Eq. (3), the trend in the predicted thermal conductivity vs. thickness is similar to that predicted via Eq. (2), as seen by the black dashed line in the inset of Figure 6, but it provides a slightly different result for the intrinsic thermal conductivity of our of open atmosphere-grown Ga_2O_3 ($\kappa = 8.0 \pm 2.3$ W m^{-1} K^{-1}), because the thickness-dependencies typical in size effects of the thermal conductivity of films are not necessarily one-to-one correlated with the thermal boundary conductance across solid interfaces.[47,48] Stated differently, the thermal boundary conductance cannot fully account for the size effects in thermal conductivity. Future studies on size effects in the thermal conductivity and

thermal boundary conductance across solid interfaces that are focused on more ideal, traditionally studied nanomaterial systems should be pursued to elucidate the relationship between phonon-boundary scattering, its effects on the reduction in thermal conductivity, and its contribution to thermal transport across solid/solid interfaces. Furthermore, for applications of our material systems, the concern lies in the total thermal resistance that the β-Ga_2O_3 film adds to heat flow from the metal contact into the GaN layer.

Taking an average of the results from both approaches to model the thickness dependence in the thermal conductivity of β-Ga_2O, we therefore report that the intrinsic thermal conductivity of β-Ga_2O_3 grown via open-atmosphere annealing of GaN is $8.8 \pm 3.4\,W\,m^{-1}\,K^{-1}$. This thermal conductivity is slightly lower than a previous measurement of the thermal conductivity of bulk, single crystalline β-Ga_2O_3 ($\sim 13\,W\,m^{-1}\,K^{-1}$—black dotted line in Fig. 6),[49,50] and roughly half the value of the thermal conductivity of typical GaN HFET component AlGaN ($16.6\,W\,m^{-1}\,K^{-1}$).[51] Given the polycrystalline nature of our β-Ga_2O_3 films, this reduction in thermal conductivity relative to the single crystalline value reported in Ref. 49 is not surprising. Similarly, the defects in our films arising from our method of synthesis and clearly observed in our TEM images in Fig. 1 would also lead to a reduction in thermal conductivity compared to higher quality, single crystalline β-Ga_2O_3. Although the intrinsic thermal conductivity of our β-Ga_2O_3 is nearly an order of magnitude larger than the other typical gate insulators shown in Fig. 6 (amorphous SiO_2 and SiN_x), boundary effects are pronounced enough that for typical gate oxide thicknesses, the effective thermal conductivity is reduced to similar values as these gate dielectric materials.

We attribute the relatively large variation in measured thermal conductivity (both from the analytical models and among the samples with different metal transducers) at larger β-Ga_2O_3 thicknesses to fluctuations in roughness as a consequence of the relatively simple growth method used to produce β-Ga_2O_3. The samples were annealed in a tube furnace open to the atmosphere until the desired roughness was achieved. As shown in Figure 1, this can produce a violent interface between the substrate and the growth, resulting in inconsistent interfacial properties. Therefore, some of our specific samples are not ideally modeled with the simplified analytical approach applied to the data in Fig. 6. However, with our rigorous uncertainty analysis, this model gives appropriate insight into the thermal properties of open-atmosphere grown β-Ga_2O_3.

The opportunity for thermal benefits in GaN devices arises in manipulating the thermal boundary conductance across the β-Ga_2O_3/GaN interface. As previously mentioned, using Eq. (2) and the previous-discussed assumptions associated with this, we determined h_K across this interface as $31.2 \pm 8.1\,MW\,m^{-2}\,K^{-1}$. This is on the same order as the room temperature thermal boundary conductances reported for SiO_2/Si interfaces ($h_K = 50\,MW\,m^{-2}\,K^{-1}$)[42] and dislocation dense GaSb/GaAs interfaces grown epitaxially ($h_K = 10$–$20\,MW\,m^{-2}\,K^{-1}$).[52] Our TEM and STEM analyses shown in Fig. 1 indicate the "imperfect" nature of the boundary between the β-Ga_2O_3 and GaN, which can lead to large reductions in thermal boundary conductance.[6] Given this relatively low conductance (large resistance) associated with this interface compared to the intrinsic thermal conduction mechanisms in bulk β-Ga_2O_3, the opportunity exists to engineer this interface and thereby increase the overall thermal conduction across a metal/β-Ga_2O_3/GaN junction.

The possibility of increasing the thermal conductance across metal/β-Ga_2O_3/GaN junctions has tremendous implications for thermal mitigation of GaN-based devices by engineering hot spots around gate regions. Beta-phase Ga_2O_3 is easily grown on GaN via thermal oxidation, and it has many of the necessary electronic characteristics to be used as a gate oxide: low density of states at the β-Ga_2O_3/GaN interface,[53] high breakdown field,[53] high dielectric constant,[53] and wide band gap.[54] Although, the β-Ga_2O_3/GaN valence and conduction band offsets are low: 1.4 eV and 0.1 eV, respectively,[55] compared to 4.4 eV and 3.4 eV for SiO_2/Si,[56] which could lead to increased leakage current. Furthermore, β-Ga_2O_3 is very chemically stable, even in concentrated acids,[57] which could be problematic or promotional for chemical etching procedures depending on what the end goal is. Thus, further chemical and electronic research is necessary to realize the full potential of β-Ga_2O_3 as a gate dielectric. However, this issue is outside the scope of this study; our focus is thermal characterization. Our thermal measurements of open atmosphere-grown β-Ga_2O_3 demonstrate the intrinsically larger thermal conductivity and mean free paths compared to typical amorphous gate dielectrics, indicating the possibility for increased thermal spreading of heat from localized hot spots at gate/channel contacts compared to typical dielectric and passivation layers. This makes annealing of GaN to form surface layers of β-Ga_2O_3 a promising candidate for gate dielectrics and other surface passivation layers in next generation GaN devices.

V. SUMMARY

Our work reports on the size effects of the thermal conductivity of beta-phase gallium oxide (β-Ga_2O_3) thin films, a component of typical gate oxides used in such devices. We use time domain thermoreflectance to measure the thermal conductivity of a variety of polycrystalline β-Ga_2O_3 films of different thicknesses grown via open atmosphere annealing of GaN surfaces. We confirm that the β-Ga_2O_3 grown from annealing the GaN surface is phase-pure, and varies in both surface roughness and diffusion into the GaN based on annealing time. The effective thermal conductivity of β-Ga_2O_3 can span 1.5 orders of magnitude, increasing with an increased film thickness, which is indicative of the relatively large intrinsic thermal conductivity of bulk β-Ga_2O_3 ($8.8 \pm 3.4\,W\,m^{-1}\,K^{-1}$) and large mean free paths compared to typical gate dielectrics commonly used in GaN device contacts. By conducting TDTR measurements with different metal transducers (Al, Au, and Au with a Ti wetting layer), we attribute this variation in effective thermal conductivity to a combination of size effects in the β-Ga_2O_3 film resulting from phonon scattering at the β-Ga_2O_3/GaN interface and thermal transport across the β-Ga_2O_3/GaN interface. From our measurements and assuming a series resistor model, we

quantify the thermal boundary conductance across the β-Ga_2O_3/GaN interface as $31.2 \pm 8.1\,MW\ m^{-2}\ K^{-1}$, in the range of typical thermal boundary conductances previously observed non-metal/non-metal interfaces. The measured thermal properties of open atmosphere-grown β-Ga_2O_3 and its interface with GaN set the stage for thermal engineering of gate contacts in high frequency GaN-based devices.

ACKNOWLEDGMENTS

The material is based upon work partially supported by the Air Force Office of Scientific Research under AFOSR Award No. FA9550-14-1-0067 (Subaward No. 5010-UV-AFOSR-0067), the National Science Foundation (CBET-1339436) and the Commonwealth Research Commercialization Fund (CRCF) of Virginia.

[1]D. G. Cahill, P. V. Braun, G. Chen, D. R. Clarke, S. Fan, K. E. Goodson, P. Keblinski, W. P. King, G. D. Mahan, A. Majumdar, H. J. Maris, S. R. Phillpot, E. Pop, and L. Shi, "Nanoscale thermal transport. II. 2003–2012," Appl. Phys. Rev. **1**, 011305 (2014).
[2]D. G. Cahill, W. K. Ford, K. E. Goodson, G. D. Mahan, A. Majumdar, H. J. Maris, R. Merlin, and S. R. Phillpot, "Nanoscale thermal transport," J. Appl. Phys. **93**, 793–818 (2003).
[3]G. Chen, *Nanoscale Energy Transport and Conversion: A Parallel Treatment of Electrons, Molecules, Phonons, and Photons* (Oxford University Press, New York, 2005).
[4]E. T. Swartz and R. O. Pohl, "Thermal boundary resistance," Rev. Mod. Phys. **61**, 605–668 (1989).
[5]P. L. Kapitza, "The study of heat transfer in Helium II," Zh. Eksp. Teor. Fiz. **11**, 1–31 (1941).
[6]P. E. Hopkins, "Thermal transport across solid interfaces with nanoscale imperfections: Effects of roughness, disorder, dislocations, and bonding on thermal boundary conductance," ISRN Mech. Eng. **2013**, 682586 (2013).
[7]E. Pop, "Energy dissipation and transport in nanoscale devices," Nano Res. **3**, 147–169 (2010).
[8]A. N. Smith and J. P. Calame, "Impact of thin film thermophysical properties on thermal management of wide bandgap solid-state transistors," Int. J. Thermophys. **25**, 409–422 (2004).
[9]R. J. Trew, "SiC and GaN transistors—Is there one winner for microwave power applications?," Proc. IEEE **90**, 1032–1047 (2002).
[10]S.-M. Lee, D. G. Cahill, and T. H. Allen, "Thermal conductivity of sputtered oxide films," Phys. Rev. B **52**, 253–257 (1995).
[11]R. M. Costescu, A. J. Bullen, G. Matamis, K. E. O'Hara, and D. G. Cahill, "Thermal conductivity and sound velocities of hydrogen-silsequioxane low-k dielectrics," Phys. Rev. B **65**, 094205 (2002).
[12]C. S. Gorham, J. T. Gaskins, G. N. Parsons, M. D. Losego, and P. E. Hopkins, "Density dependence of the room temperature thermal conductivity of atomic layer deposition grown amorsphous alumina (Al2O3)," Appl. Phys. Lett. **104**, 253107 (2014).
[13]J. W. Johnson, B. Luo, F. Ren, B. P. Gila, W. Krishnamoorthy, C. R. Abernathy, S. J. Pearton, J. I. Chyi, T. E. Nee, C. M. Lee, and C. C. Chuo, "Gd_2O_3/GaN metal-oxide-semiconductor field-effect transistor," Appl. Phys. Lett. **77**, 3230 (2000).
[14]T. D. Lin, H. C. Chiu, P. Chang, L. T. Tung, C. P. Chen, M. Hong, J. Kwo, W. Tsai, and Y. C. Wang, "High-performance self-aligned inversion-channel $In_{0.53}Ga_{0.47}As$ metal-oxide-semiconductor field-effect-transistor with $Al_2O_3/Ga_2O_3(Gd_2O_3)$ as gate dielectrics," Appl. Phys. Lett. **93**, 033516 (2008).
[15]F. Ren, M. Hong, S. N. G. Chu, M. A. Marcus, M. J. Schurman, A. Baca, S. J. Pearton, and C. R. Abernathy, "Effect of temperature on $Ga_2O_3(Gd_2O_3)$/GaN metal-oxide-semiconductor field-effect transistors," Appl. Phys. Lett. **73**, 3893 (1998).
[16]V. R. Reddy, M. Ravinandan, P. K. Rao, and C.-J. Choi, "Effects of thermal annealing on the electrical and structural properties of Pt/Mo Schottky contacts on n-type GaN," J. Mater. Sci. Mater. Electron. **20**, 1018 (2009).
[17]W. Cao and S. K. Dey, "Microstructure and properties of sol-gel derived $Pb(Zr_{0.3}Ti_{0.7})O_3$ thin films on GaN/sapphire for nanoelectromechanical systems," J. Sol-Gel Sci. Technol. **42**, 389 (2007).
[18]A. Y. Polyakov, N. B. Smirnov, A. V. Govorkov, A. A. Shlensky, and S. J. Pearton, "Influence of high-temperature annealing on the properties of Fe doped semi-insulating GaN structure," J. Appl. Phys. **95**, 5591 (2004).
[19]Y. Hayashi, R. Hasunuma, and K. Yamabe, "Generation and growth of atomic-scale roughness at surface and interface of silicon dioxide thermally grown on atomically flat Si surface," Key Eng. Mater. **470**, 110 (2011).
[20]H. Döscher, G. Lilienkamp, P. Iskra, M. Kazempoor, and W. Daum, "Thermal stability of thin ZrO_2 films prepared by a sol-gel process on Si (001) substrates," J. Vac. Sci. Technol. B **28**, C5B5 (2010).
[21]Y. Dong, R. M. Feenstra, and J. E. Northrup, "Oxidized GaN(0001) surfaces studied by scanning tunneling microscopy and spectroscopy and by first-principles theory," J. Vac. Sci. Technol. B **24**, 2080 (2006).
[22]C. J. Lu, A. V. Davydov, D. Josell, and L. A. Bendersky, "Interfacial reactions of Ti/*n*-GaN contacts at elevated temperature," J. Appl. Phys. **94**, 245 (2003).
[23]B. P. Luther, S. E. Mohney, T. N. Jackson, M. A. Khan, Q. Chen, and J. W. Yang, "Investigation of the mechanism for Ohmic contact formation in Al and Ti/Al contacts to *n*-type GaN," Appl. Phys. Lett. **70**, 57 (1997).
[24]S. S. Kumar, E. J. Rubio, M. Noor-A-Alam, G. Martinez, S. Manandhar, V. Shutthanandan, S. Thevuthasan, and C. V. Ramana, "Structure, morphology, and optical properties of amourphous and nanocrystalline gallium oxide thin films," J. Phys. Chem. **117**, 4194 (2013).
[25]Y. Lv, L. Yu, G. Zha, D. Zheng, and C. Jiang, "Application of soluble salt-assisted route to synthesis of β-Ga_2O_3 nanopowders," Appl. Phys. A: Mater Sci. Process. **114**, 351 (2014).
[26]X. A. Cao, S. J. Pearton, G. Dang, A. P. Zhang, F. Ren, and J. M. Van Hove, "Effects of interfacial oxides on Schottky barrier contacts to *n*- and *p*-type GaN," Appl. Phys. Lett. **75**, 4130 (1999).
[27]K. Prabhakaran, T. G. Andersson, and K. Nozawa, "Nature of native oxide on GaN surface and its reaction with Al," Appl. Phys. Lett. **69**, 3212 (1996).
[28]G. T. Hohensee, W.-P. Hsieh, M. D. Losego, and D. G. Cahill, "Interpreting picosecond acoustics in the case of low interface stiffness," Rev. Sci. Instrum. **83**, 114902 (2012).
[29]C. Thomsen, J. Strait, Z. Vardeny, H. J. Maris, J. Tauc, and J. J. Hauser, "Coherent phonon generation and detection by picosecond light pulses," Phys. Rev. Lett. **53**, 989–992 (1984).
[30]D. G. Cahill, K. Goodson, and A. Majumdar, "Thermometry and thermal transport in micro/nanoscale solid-state devices and structures," J. Heat Transfer **124**, 223 (2002).
[31]P. E. Hopkins, J. R. Serrano, L. M. Phinney, S. P. Kearney, T. W. Grasser, and C. T. Harris, "Criteria for cross-plane dominated thermal transport in multilayer thin film systems during modulated laser heating," J. Heat Transfer **132**, 081302 (2010).
[32]A. J. Schmidt, X. Chen, and G. Chen, "Pulse accumulation, radial heat conduction, and anisotropic thermal conductivity in pump-probe transient thermoreflectance," Rev. Sci. Instrum. **79**, 114902 (2008).
[33]D. G. Cahill, "Analysis of heat flow in layered structures for time-domain thermoreflectance," Rev. Sci. Instrum. **75**, 5119 (2004).
[34]R. Rosei, "Temperature modulation of the optical transitions involving the Fermi surface in Ag: Theory," Phys. Rev. B **10**, 474 (1974).
[35]R. Rosei, C. H. Culp, and J. H. Weaver, "Temperature modulation of the optical transitions involving the Fermi surface in Ag: Experimental," Phys. Rev. B **10**, 484 (1974).
[36]R. Rosei and D. W. Lynch, "Thermomodulation spectra of Al, Au, and Cu," Phys. Rev. B **5**, 3883 (1972).
[37]R. Kremer, M. Cardona, E. Schmitt, J. Blumm, S. Estreicher, M. Sanati, M. Bockowski, I. Grzegory, T. Suski, and A. Jezowski, "Heat capacity of α-Ga N: Isotope effects," Phys. Rev. B **72**, 075209 (2005).
[38]G. B. Adams, Jr. and H. L. Johnston, "Low temperature heat capacities of inorganic solids. xi. the heat capacity of b-gallium oxide from 15 to 300°K," J. Am. Chem. Soc. **74**, 4788 (1952).
[39]G. T. Furukawa, M. L. Reilly, and J. S. Gallagher, "Critical analysis of heat—capacity data and evaluation of thermodynamic properties of ruthenium, rhodium, palladium, iridium, and platinum from 0 to 300K. A survey of the literature data on osmium," J. Phys. Chem. Ref. Data **3**, 163–209 (1974).
[40]G. T. Furukawa, W. G. Saba, and M. L. Reilly, "Critical analysis of the heat-capacity data of the literature and evaluation of thermodynamic properties of copper, silver, and gold from 0 to 300 K," DTIC Document, 1968.
[41]B. F. Donovan, C. J. Szwejkowski, J. C. Duda, R. Cheaito, J. T. Gaskins, C.-Y. P. Yang, D. L. Medlin, C. Constantin, R. E. Jones, and P. E.

Hopkins, "Thermal boundary conductance across metal-Gallium Nitride (GaN) interfaces from 80 – 450 K," Appl. Phys. Lett. **105**, 203502 (2014).
[42]S.-M. Lee and D. G. Cahill, "Heat transport in thin dielectric films," J. Appl. Phys. **81**, 2590 (1997).
[43]A. M. Marconnet, M. Asheghi, and K. E. Goodson, "From the casimir limit to phononic crystals: 20 years of phonon transport studies using silicon-on-insulator technology," ASME J. Heat Transfer **135**, 061601 (2013).
[44]B. M. Foley, H. J. Brown-Shaklee, J. C. Duda, R. Cheaito, B. J. Gibbons, D. Medlin, J. F. Ihlefeld, and P. E. Hopkins, "Thermal conductivity of nano-grained $SrTiO_3$ thin films," Appl. Phys. Lett. **101**, 231908 (2012).
[45]B. F. Donovan, B. M. Foley, J. F. Ihlefeld, J.-P. Maria, and P. E. Hopkins, "Spectral phonon scattering effects on the thermal conductivity of nano-grained barium titanate," Appl. Phys. Lett. **105**, 082907 (2014).
[46]B. Liu, M. Gu, and X. Liu, "Lattice dynamical, dielectric, and thermodynamic properties of β-Ga_2O_3 from first principles," Appl. Phys. Lett. **91**, 172102 (2007).
[47]R. Jones, J. Duda, X. Zhou, C. Kimmer, and P. Hopkins, "Investigation of size and electronic effects on Kapitza conductance with non-equilibrium molecular dynamics," Appl. Phys. Lett. **102**, 183119 (2013).
[48]S.-M. Lee and D. G. Cahill, "Influence of interface thermal conductance on the apparent thermal conductivity of thin films," Microscale Thermophys. Eng. **1**, 47–52 (1997).
[49]E. G. Villora, K. Shimamura, T. Ujiie, and K. Aoki, "Electrical conductivity and lattice expansion of β-Ga_2O_3 below room temperature," Appl. Phys. Lett. **92**, 202118 (2008).
[50]M. Handwerg, R. Mitdank, Z. Galazka, and S. F. Fischer, "Temperature-dependent thermal conductivity in Mg-doped and undoped β -Ga_2O_3 bulk-crystals," Semicond. Sci. Technol. **30**, 024006 (2015).
[51]J. Cho, Z. Li, E. Bozorg-Grayeli, T. Kodama, D. Francis, F. Ejeckam, F. Faili, M. Asheghi, and K. E. Goodson, "Improved thermal interfaces of gan-diamond composite substrates for HEMT applications," IEEE Trans. Compon., Packag., Manuf. Technol. **3**, 79–85 (2013).
[52]P. E. Hopkins, J. C. Duda, S. P. Clark, C. P. Hains, T. J. Rotter, L. M. Phinney, and G. Balakrishnan, "Effect of dislocation density on thermal boundary conductance across GaSb/GaAs interfaces," Appl. Phys. Lett. **98**, 161913 (2011).
[53]C.-T. Lee, H.-W. Chen, and H.-Y. Lee, "Metal–oxide–semiconductor devices using Ga_2O_3 dielectrics on n-type GaN," Appl. Phys. Lett. **82**, 4304–4306 (2003).
[54]M. D. Losego, *Interfacing epitaxial oxides to gallium nitride*, North Carolina State University, 2008, p. 249.
[55]W. Wei, Z. Qin, S. Fan, Z. Li, K. Shi, Q. Zhu, and G. Zhang, "Valence band offset of b-Ga_2O_3/wurtzite GaN heterostructure measured by X-ray photoelectron spectroscopy," Nanoscale Res. Lett. **7**, 562 (2012).
[56]A. Alkauskas, P. Broqvist, F. Devynck, and A. Pasquarello, "Band offsets at semiconductor-oxide interfaces from hybrid density-functional calculations," Phys. Rev. Lett. **101**, 106802 (2008).
[57]M. Passlack, E. F. Schubert, W. S. Hopson, M. Hong, N. Moriya, S. N. G. Chu, K. Konstadinidis, J. P. Mannaerts, M. L. Schnoes, and G. J. Zydzik, "Ga_2O_3 films for electronic and optoelectronic applications," J. Appl. Phys. **77**, 686 (1995).